coatings

MDPI

Article

Effect of Cerium Tartrate on the Corrosion Resistance of Epoxy Coating on Aluminum Alloy and Its Mechanism

Xueping Chen [1], Jianhua Tang [1], Han Wei [1], Hanlu Zhang [2], Yuming Tang [1,*], Xuhui Zhao [1,*] and Yu Zuo [1]

[1] Beijing Key Laboratory of Electrochemical Process and Technology for Materials, Beijing University of Chemical Technology, Beijing 100029, China; 18811651858@163.com (X.C.); tangjianhua0708@163.com (J.T.); 2019210177@buct.edu.cn (H.W.); zuoy@mail.buct.edu.cn (Y.Z.)
[2] No.92228 of the People's Liberation Army, Beijing 100072, China; zhanghanlu_123@163.com
* Correspondence: tangym@mail.buct.edu.cn (Y.T.); xhzhao@mail.buct.edu.cn (X.Z.)

Abstract: The inhibition effect and mechanism of cerium tartrate (CeTar) as a pigment in epoxy coating on AA2024-T3 aluminum alloy in 3.5% NaCl solution were studied. Two kinds of coatings were applied on the substrate, including a single-layer epoxy coating with CeTar distributed uniformly and a double-layer coating composed of an inner layer doped with CeTar and an outer layer with no CeTar. The protective performances of the coatings were assessed by a Machu test and an Electrochemical impedance spectroscopy (EIS) technique. The corrosion inhibition mechanism of CeTar in the coating was analyzed with X-ray photoelectron spectroscopy (XPS), inductively coupled plasma mass spectrometry (ICP-MS) and Fourier transform spectroscopy (FTIR). The results show that the addition of CeTar can evidently improve the protective performance of the epoxy coating for a long time (>520 d). This might have relationship with the modification effect on the epoxy coating by cerium salts, and also may be due to the synergistic inhibitory effect by tartrate group and cerium ions on the alloy substrate after their continuous releasing to the coating/alloy interface and forming of a protective film. The double-layer coating provides similar protective properties to the single-layer coating. This suggested that creating a protective film on the aluminum alloy substrate could result in a greater contribution to improving the protection performance of the coating.

Keywords: cerium tartrate; epoxy coating; aluminum alloy; corrosion protection; EIS

Citation: Chen, X.; Tang, J.; Wei, H.; Zhang, H.; Tang, Y.; Zhao, X.; Zuo, Y. Effect of Cerium Tartrate on the Corrosion Resistance of Epoxy Coating on Aluminum Alloy and Its Mechanism. *Coatings* **2022**, *12*, 785. https://doi.org/10.3390/coatings12060785

Academic Editors: Claudia Barile and Gilda Renna

Received: 17 April 2022
Accepted: 5 June 2022
Published: 7 June 2022

1. Introduction

AA2024-T3 aluminum alloy, which has excellent mechanical properties such as high strength-to-weight ratio, low density and good electrical conductivity, is widely used in aerospace and other industries. However, the aluminum alloy is sensitive to localized corrosion when exposed to aggressive environments because of the intermetallic particles in the alloy [1]. Chromate-containing coatings are effectively applied for the protection of metals, due to their combined inhibition to both anodic and cathodic reactions occurring on the metals. However, chromates have been banned for their carcinogenicity and toxicity, so there is an urgent need to develop environmentally friendly corrosion inhibitors to replace chromates for protecting aluminum alloys [2–4].

Hinton et al. found that the rare earth salts, such as $CeCl_3$, $LaCl_3$ and YCl_3, exhibit very good corrosion inhibitory effect on AA7075 aluminum alloy [5,6]. Among of them, cerium salts are considered to be one of the most effective inhibitors [7–9]. The corrosion rate of the Al alloy is decreased because of a cerium oxide/hydroxides film being formed, inhibiting the cathodic oxygen reduction reaction [10–12]. Tiringer et al. [13] incorporated cerium nitrate ($Ce(NO_3)_3$) into a sol-gel coating and pointed out that $Ce(NO_3)_3$ could improve the corrosion resistance of the AA7075-T6 aluminum alloy and enhance the self-healing ability of the coating. Generally, inorganic cerium salts, such as $Ce(NO_3)_3$ and $CeCl_3$, have high solubilities, therefore they are easily released from organic coatings. This does not

contribute to the long-term stability of the coating. Organic cerium salts possess relatively lower solubilities and, acting as mixed inhibitors, they can suppress both the anodic and cathodic processes on some metals and alloys [11]. This gives them the theoretical basis for being added into organic coatings as pigments [14–17]. Shi et al. [14] studied the corrosion protection of AA2024-T3 aluminum alloy in 0.05 M NaCl solution by cerium cinnamate (CeCin) and pointed out that CeCin mainly acts as an anodic inhibitor during the initial immersion time and acts as a cathodic inhibitor during the later immersion time. Mardel et al. [18] investigated the protective effect of cerium dibutyl phosphate ($Ce(dbp)_3$) in the epoxy coating on 2024-T3 aluminum alloy. The results showed that although $Ce(dbp)_3$ can improve the water absorption of the coating, cerium ions are slowly released from the coating and effectively slow down filiform corrosion. The corrosion inhibitory effect of organic cerium salts in organic coating has a close relationship with the release of Ce^{3+} to the metallic substrate. Soestbergen et al. [16] studied the leaching behaviors of $Ce(dbp)_3$ with different loadings in epoxy coatings and pointed out that a porous network might be formed in the highly $Ce(dbp)_3$ loaded coatings and benefits from a constant release of Ce^{3+}.

In addition to the corrosion inhibition on the substrate, the rare earth salts also have a positive effect on the epoxy network. Jouyandeh et al. [19–21] studied the influence of lanthanide-doped nanoparticles on the curing process of epoxy and reported that Sm^{3+} and Cd^{3+} cations participate in the cross-linking of epoxy, resulting in a denser cross-linked network. Tiringer et al. [13] and Mardel et al. [18] also pointed out that Ce ions promote organic polymerization of the network and the process of epoxy ring opening. Cerium tartrate (CeTar) also can be used as pigments in organic coatings. Hu et al. [22] added 2 wt%, 5 wt% and 15 wt% of CeTar to an epoxy coating and found that the coating containing 15 wt% CeTar shows the best corrosion resistance to the 2024-T3 aluminum alloy. Being a both cathodic and anodic inhibitor, CeTar could improve the corrosion and protection property of the coatings through a combined action of cerium ions and organic groups [22,23].

Although previous works have revealed the performance improvement mechanism of CeTar to epoxy coatings, the testing data are relatively short. In practice, organic coatings are supposed to provide long-term service. Therefore, it is good to understand the long-term corrosion and protection behavior of organic coatings. In this work, electrochemical impedance spectroscopy (EIS) was used to evaluate the protective ability of an epoxy coating with CeTar powders to the AA2024 aluminum alloy in 3.5% NaCl solution for 520 d. Considering the cost of CeTar and the inhibitory effect of the cerium salt, which is likely related to the protection effect on the substrate, a double-layer epoxy coating was prepared, in which CeTar powders were only added into the inner layer that contacting with the substrate. The cerium ion release and the effect of CeTar on the structure of the epoxy coating were investigated by inductively coupled plasma mass spectrometry (ICP-MS) and Fourier transform infrared spectroscopy (FTIR). The inhibition mechanism of CeTar on Al alloy substrate was analyzed by X-ray photoelectron spectroscopy (XPS) test.

2. Experimental

2.1. Materials and Samples Preparation

The substrate used was 2024-T3 aluminum alloy, which has the nominal composition (wt%): Si 0.5, Fe 0.5, Cu 3.8, Mn 0.9, Mg 1.8, Ni 0.1, Zn 0.25, Al Balance. The panel was cut to 50 mm × 50 mm × 2 mm specimen, then the surface was sanded with 120# sandpaper, cleaned with ethanol and acetone, and finally dried sufficiently in air before the coating was applied.

Cerium tartrate (CeTar) powders were prepared by the reaction of sodium tartrate and cerium nitrate. They were supplied by Fuchen Chemical Reagent Co., Ltd. (Tianjin, China), and Beijing Chemical Reagent Co., Ltd. (Beijing, China), respectively. The process and details have been provided in the literature [24]. The preparation process of coating is as follows. Firstly, a diluent was prepared by mixing n-butanol and xylene at a mass ratio

of 7:3. Then, some of the diluent was added into a E-44 epoxy resin (Dai's Zed Technology Development Co., Ltd., Beijing, China) to prepare a resin solution. The other part of diluent was mixed with CeTar powders and ultra-sonicated for 30 min, and then mixed with the epoxy resin solution, stirring for 30 min. Finally, a T-31 amine curing agent (Dai's Zed Technology Development Co., Ltd., Beijing, China) was added and stirred for 10 min to prepare the coating. The mass ratio was 2.5:1 for E-44 and T-31.

Two kinds of epoxy coating samples were prepared on 2024-T3 aluminum alloy substrate by a manual brushing method, including single-layer coating and double-layer coating samples, seen in Figure 1. The single-layer coating meant a coating in which CeTar powders dispersed in the whole coating with 60 ± 5 μm dry film thickness. The double-layer coating consisted of 2 coating layers, in which an inner layer containing CeTar powders was applied to the substrate firstly, then after 2 h an outer epoxy varnish layer without CeTar was applied. The thickness of each layer is 30 μm. After brushed, the coatings were cured for 7 d at room temperature. The dry film thickness was measured with a TT230 coating thickness gauge (KODIN, Beijing, China).

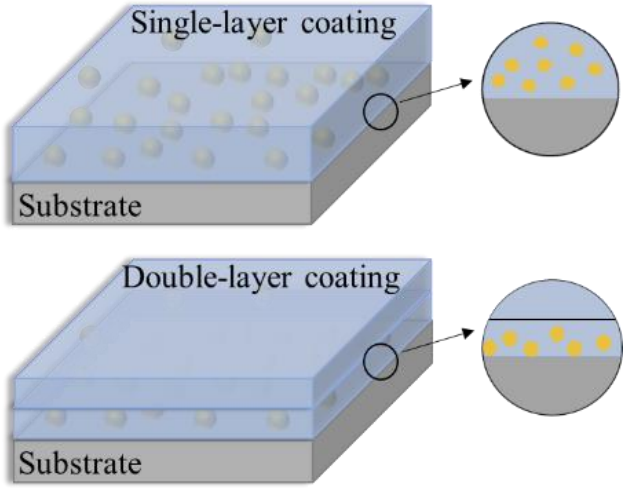

Figure 1. The diagram of two kinds of coating samples prepared.

2.2. Experimental Methods

A Machu test was employed to quickly evaluate the corrosion prevention performance of the coatings [25–28]. Before the test, the coated panels were scratched with a razor blade to produce cross lines with width of 0.3–1.0 mm, then were immersed into a solution (37 °C) of 5 mL/L H_2O_2 (30 vol%) + 50 g/L NaCl. After 48 h of immersion, the panels were taken out and the corrosion morphology was observed.

The samples with no cross-scribed scratch coating were immersed in 3.5% NaCl solution. An electrochemical impedance spectroscopy (EIS) test was performed on the samples by a PARSTAT 2273 instrument (Princeton, Oak Ridge, TN, USA) regularly. A three-electrode cell was used, in which a saturated calomel electrode was reference electrode, a platinum electrode was auxiliary electrode and the coated sample with a 10 cm^2 exposed area was working electrode. The test solution was a 3.5% NaCl solution (room temperature). Prior to EIS test, the sample was immersed in solution for at least 10 min to obtain a stable open circuit potential. The amplitude of sinusoidal voltage signal was 10 mV, and the scanning frequency range was 10^5~10^{-2} Hz. Under each condition, four parallel samples were used. Zsimpwin software (V 3.50, San Diego, CA, USA) was used to analyze EIS data.

An inductively coupled plasma mass spectrometer (ICP-MS, Agilent Technologies 7700 series, Palo Alto, CA, USA) was used to quantitatively detect the contents of cerium ions in 3.5% NaCl solution in which the coated samples were immersed, in order to monitor

the release of the cerium from the coating. The release rate of cerium ions was calculated by Formula (1) [29]:

$$R = \rho \times V \times 24/(t \times A) \quad (1)$$

where, R was the release rate (μg/(cm^2·d)), ρ was the cumulative concentration of cerium ions in solution (μg/L), V was the solution volume (10 mL), A was the test area of the coated sample (10 cm^2), and t testing time (h).

The chemical functional groups in the coating were analyzed by a TENSOR27 infrared spectrometer (BRUKER, Karlsruhe Germany). The measuring range was 500–4000 cm^{-1}. The morphology of the coating was observed by a scanning electron microscope (XL30 ESEM, Philips, Amsterdam, The Netherlands) and the elements were analyzed with a X-ray energy spectrometer (EDS, NORAN Vantage, Thermo Scientific, Waltham, MA, USA). The surface composition of the AA2024 alloy substrate was analyzed by a ESCALAB 250 X-ray photoelectron spectroscopy (XPS) (ESCALAB 250, Thermo VG, Waltham, MA, USA). Before the measurement, the sample was soaked in a N,N-dimethylformamide solution solvent (25 °C, 24 h) to get the coating removed from the substrate. Avantage software (V 5.948, Waltham, MA, USA) was used to fit the XPS spectra.

3. Results and Discussion

3.1. The Distribution of Cerium Tartrate in the Epoxy Coating

Figure 2a shows the microscopic morphology of the cross-section of the single-layer epoxy coating containing 5 wt% of cerium tartrate (CeTar). It can be observed that white particles are uniformly distributed in the coating with the diameter of less than 1–10 μm. A Ce EDS mapping image is shown in Figure 2b. Figure 2c,d present an enlarged image of the white particles and the EDS result. The main components are Ce (4.28 wt%), C (76.94 wt%) and O (18.78 wt%), which indicates that the white particles are composed of cerium tartrate. These results prove that cerium tartrate salts are doped and uniformly distributed in the epoxy coating.

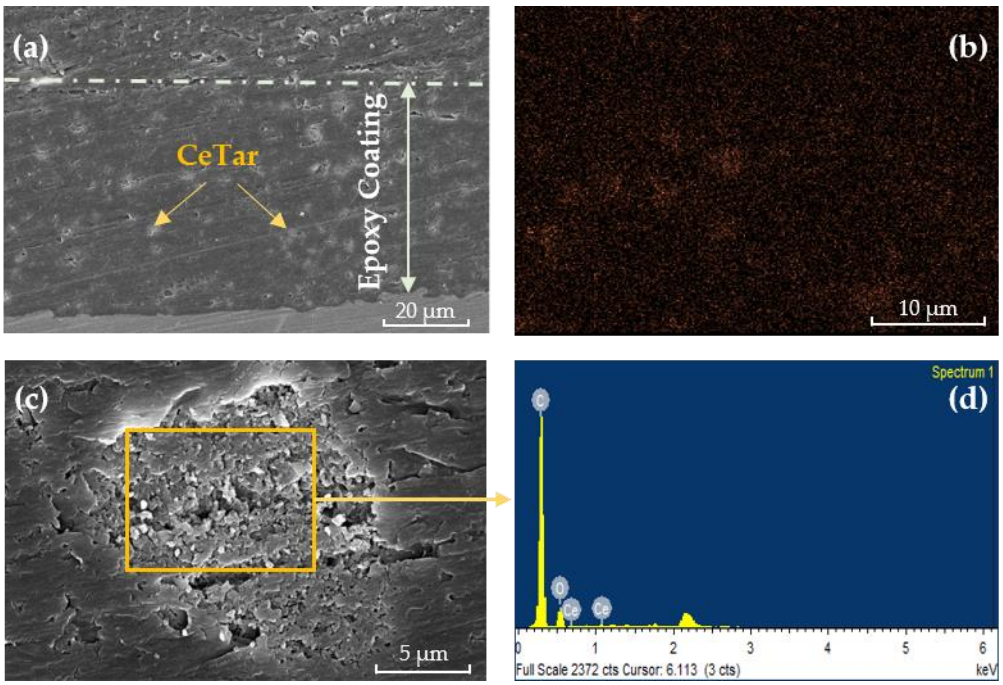

Figure 2. Cross-sectional SEM images and EDS results of the epoxy coating containing CeTar: (**a**) cross-sectional SEM image; (**b**) Ce EDS mapping image; (**c**) enlarged image of white particles; (**d**) EDS result of white particles.

3.2. Effect of Cerium Tartrate on the Protective Performance of the Epoxy Coating

Different contents of CeTar (0 wt%, 1.5 wt%, 3 wt% and 5 wt%) were added into the epoxy coatings and Machu test was employed to quickly evaluate the effect of the CeTar content on the corrosion prevention property of the coatings. Figure 3 presents the digital photos of the coating samples with different CeTar contents after 48 h Machu test. After CeTar was added, the coating presents orange-yellow color, which confirms the existence of cerium salts. For the coating without CeTar in Figure 3a, many blisters are observed around the cross scribes and part of the coating has peeled off, and the substrate on the scribe lines are severely corroded. The samples containing 1.5 wt% and 3 wt% CeTar (Figure 3b,c) also present blistering at the scratches, but the disbonding effect of the coating is relatively a little lighter. For the coating containing 5 wt% CeTar (Figure 3d), no apparent blistering and corrosion are observed. So, in the following study, addition of 5 wt% CeTar were selected.

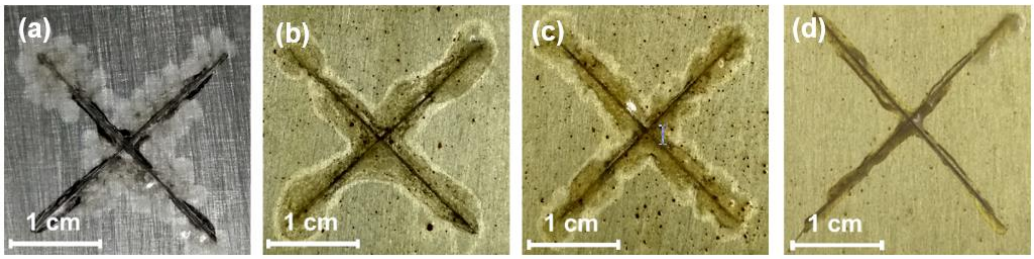

Figure 3. Photos of the coating samples containing different contents of CeTar after 48 h Machu test: (**a**) 0 wt% CeTar; (**b**) 1.5 wt% CeTar; (**c**) 3 wt% CeTar; (**d**) 5 wt% CeTar.

An EIS test is a non-destructive testing method which can be used to study the electrochemical behaviors and evaluate the barrier properties of the coatings for long time. Figure 4 shows the EIS spectra of the coating samples with different contents (0 wt%, 1.5 wt%, 3 wt% and 5 wt%) of CeTar for various immersion time. The low-frequency impedance ($|Z|_{0.01\ Hz}$) was used to compare the barrier properties of the coatings, and the results are shown in Figure 5. It can be seen that the $|Z|_{0.01\ Hz}$ values of all the samples rapidly decrease in the first period of 5 d, probably due to the rapid penetration of the solution into the coating. With immersion time, the $|Z|_{0.01\ Hz}$ value of the sample without CeTar decreases with a very quick speed. At 48 d, a few tiny blisters appear on the coating and meanwhile the value of $|Z|_{0.01\ Hz}$ decreases to $1.3 \times 10^7\ \Omega{\cdot}cm^2$. At 85 d, many blisters are observed on a large-scale area of the coating surface, indicating an obvious failure of the coating. At this time, the $|Z|_{0.01\ Hz}$ modulus decreases to $9.0 \times 10^5\ \Omega{\cdot}cm^2$. The decreasing tendency of the $|Z|_{0.01\ Hz}$ for the coating containing 1.5 wt% CeTar is similar to that of the pure epoxy coating. After 130 d immersion, the value of $|Z|_{0.01\ Hz}$ decreases to $7.0 \times 10^5\ \Omega{\cdot}cm^2$ and many blisters are observed on the coating surface. The $|Z|_{0.01\ Hz}$ values of the samples containing 3 wt% and 5 wt% CeTar decrease much slowly. For the sample containing 3 wt% CeTar, after 220 d immersion obvious blisters appear on the surface of the coating, and meanwhile the $|Z|_{0.01\ Hz}$ decreases to $8 \times 10^6\ \Omega{\cdot}cm^2$. That means the coating basically loses its protective effect on the substrate. However, for the sample containing 5 wt% CeTar, even after immersing for 520 d, the $|Z|_{0.01\ Hz}$ still remains at a relative high value of $1.6 \times 10^7\ \Omega{\cdot}cm^2$, and the coating surface is basically unchanged. Therefore, the incorporation of 5 wt% CeTar can effectively improve the protection property of the epoxy coating on the aluminum alloy.

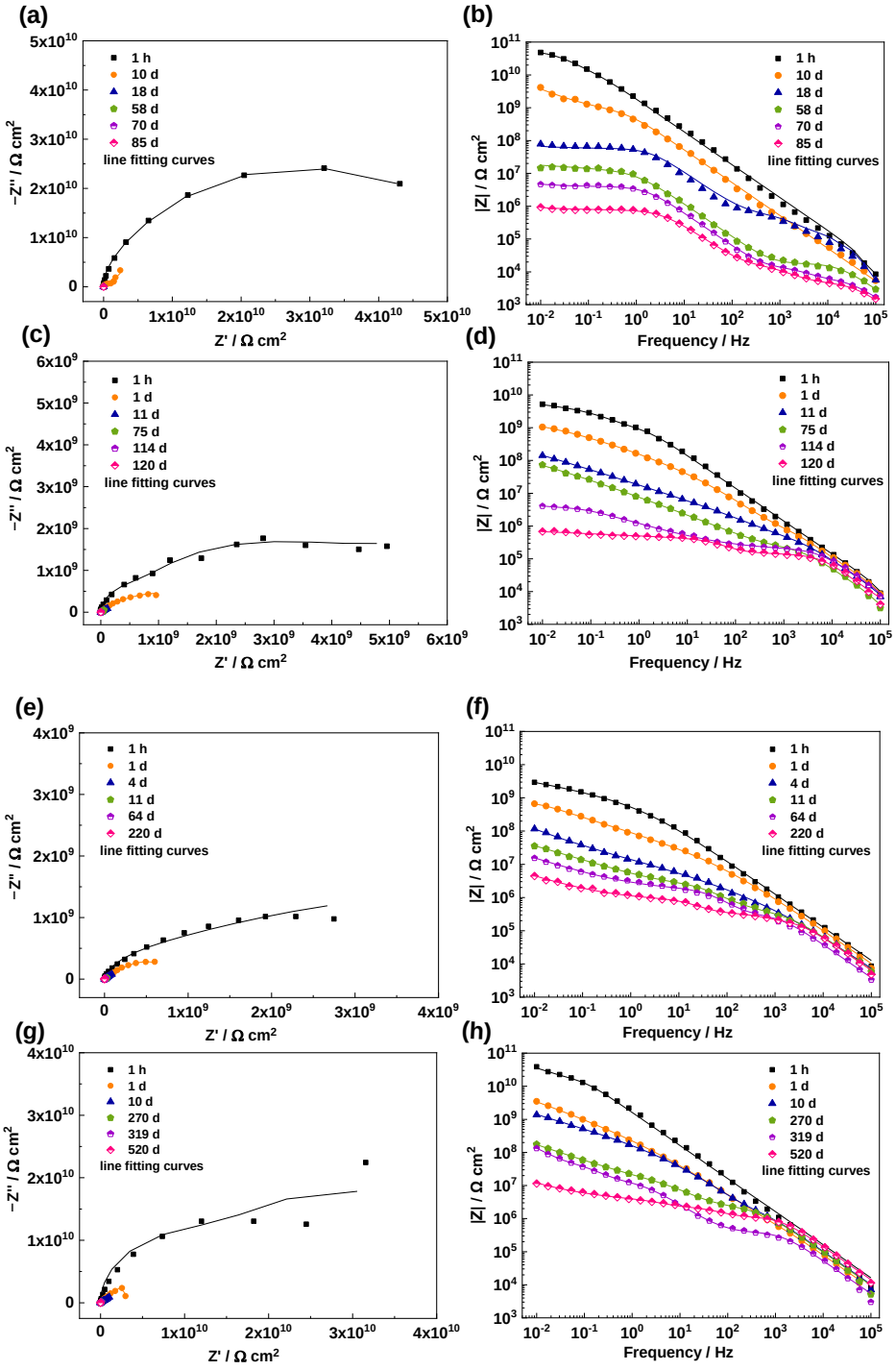

Figure 4. EIS spectra of the coated samples containing different contents of CeTar in 3.5% NaCl solution: (**a**,**b**) 0 wt% CeTar; (**c**,**d**) 1.5 wt% CeTar; (**e**,**f**) 3 wt% CeTar; (**g**,**h**) 5 wt% CeTar.

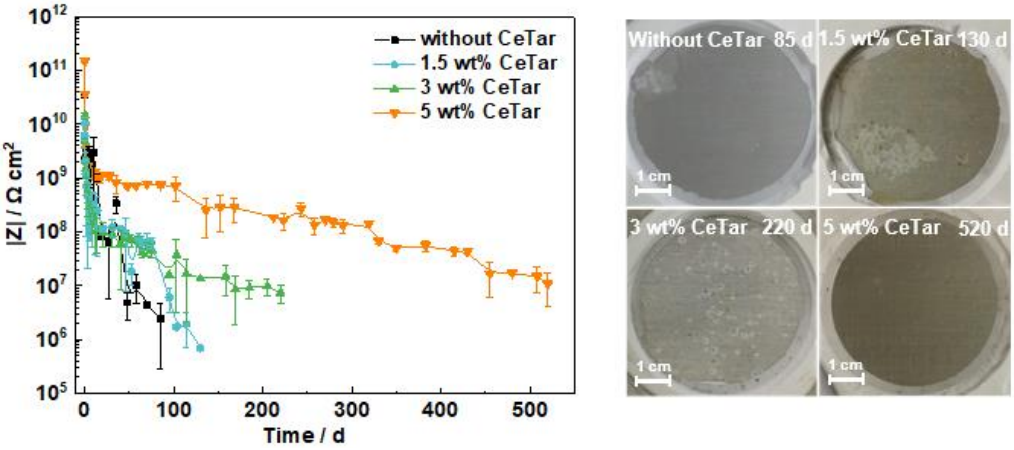

Figure 5. Variation of $|Z|_{0.01\ Hz}$ with time for the coated samples with different contents of CeTar and morphology photos of the coatings with different contents of CeTar.

3.3. EIS Analysis of Double-Layer Coated Samples Containing 5 wt% CeTar

In order to reduce the amount of the CeTar, because of its high price as pigments and in order to maintain the good protective property of the coating, a double-layer epoxy coating in which only the inner layer coating doped with 5 wt% CeTar was prepared. The protective performance of the double-layer coating was comparatively studied and compared with that of the above single-layer epoxy coating containing 5 wt% CeTar.

Figure 6 shows the photographs of double-layer coated sample before and after the Machu test. After 48 h test, no apparent delamination, blisters, or corrosion were observed, indicating that the double-layer epoxy coating containing 5 wt% CeTar in the inner layer possesses good corrosion resistance property to the aluminum alloy, which is close to that of the single-layer epoxy coating containing 5 wt% CeTar in Figure 3d.

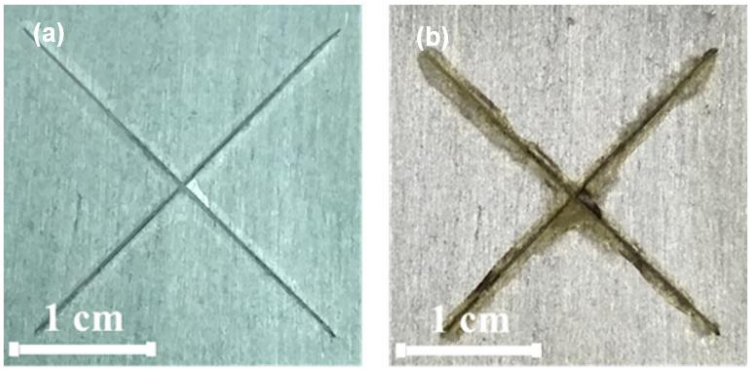

Figure 6. Photos of the double-layer coating sample before (**a**) and after (**b**) 48 h Machu test.

Figure 7 shows the EIS spectra of the double-layer coating sample immersion in 3.5% NaCl solution for 520 d. At first, the Nyquist plot presents one capacitive loop and the value of $|Z|_{0.01\ Hz}$ in the Bode plot is 3×10^{10} Ω·cm^2, manifesting a very good barrier property of the coating to the substrate. With immersion, the impedance value quickly decreases at first and then much more slowly. After immersed for 520 d, the value of $|Z|_{0.01\ Hz}$ still remains at the order of 10^7 Ω·cm^2 and no obvious blisters or rusts observed on the coating surface. This demonstrates that the double-layer coating containing 5 wt% CeTar in the inner layer also has a very good protective property to the substrate.

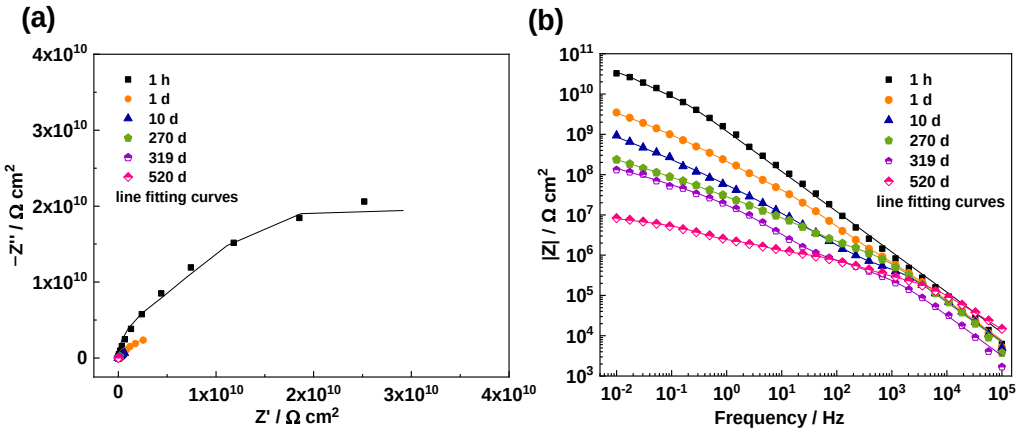

Figure 7. EIS spectra of the double-layer epoxy coatinged sample in 3.5% NaCl solution for various time: (**a**) Nyquist plot; (**b**) Bode plot.

The time-varying curves of $|Z|_{0.01\ Hz}$ for single-layer and double-layer coating samples are compared in Figure 8. Based on the variation of $|Z|_{0.01\ Hz}$, 2 kinds of coating samples exhibit no big difference in the barrier property to the substrate during 520 d immersion. This means that double-layer coating with 5 wt% CeTar in the inner layer coating presents similar protective performance with that of the single-layer coating. This result also could manifest that the protective property of the epoxy coatings with organic cerium salts is probably related to the inhibition of cerium salts on the substrate to a great extent, which aligns with the literature [18,23].

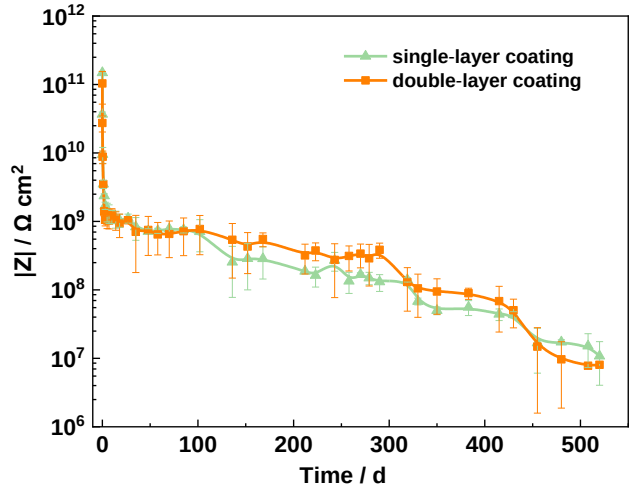

Figure 8. $|Z|_{0.01\ Hz}$ variations of single-layer and double-layer coating samples with immersion time.

The equivalent circuit models in Figure 9 were employed to analyze the EIS data of two kinds of coating samples. In which, R_c is the coating resistance, Q_c is the constant phase angle element to simulate the non-ideal capacitance behavior of the coating, Q_{dl} and R_{ct} represent the double layer capacitance and the charge transfer resistance related to the electrochemical reaction on the substrate interface, respectively, after the solution diffuses to the aluminum alloy [30,31]. When the cerium ions release from the coating and reach the surface of the aluminum, a protective film begins to form, the circuit model in Figure 9c was used, in which R_{ox} and Q_{ox} represent the resistance and capacitance associated with the protective film on the substrate. Table 1 shows the equivalent electrical circuits for the two kinds of coating samples in different immersion stages.

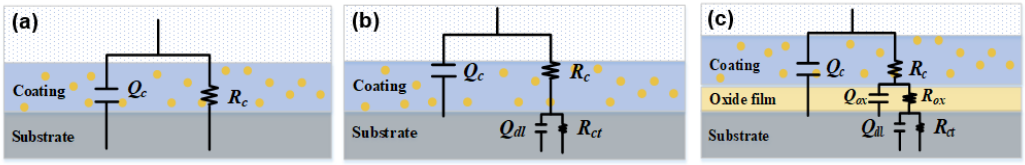

Figure 9. Equivalent circuit models for the coating samples in different immersion stages: (**a**) Model A; (**b**) Model B; (**c**) Model C.

Table 1. Equivalent circuit models for the coating samples in different immersion stages.

Coating Samples	Model A	Model B	Model C
Single-layer coating	0–5 d	6–34 d	35–520 d
Double-layer coating	0–7 d	8–26 d	27–520 d

The fitting parameters as a function of time for the two coating samples are shown in Figure 10. Figure 10a,b show the variations of Q_c and R_c. It can be seen that, more CeTar addition (single-layer coating) slightly decreases the capacitance of the coating and increases the coating resistance, indicating a slightly reduced water absorption of the coating and increased barrier property of the coating. Figure 10c,d demonstrate the variations of Q_{dl} and R_{ct} for the two coating samples. After immersion for 6 d and 8 d, the Q_{dl} and R_{ct} of single-layer coating sample and double-layer coating sample appear, respectively, which is the result of electrolyte solution penetrating through the coating to the substrate and thereby the electrochemical corrosion reaction occurring on the substrate interface. With time, the Q_{dl} increases while the R_{ct} decreases. After approximately 30 d, the variation rate of Q_{dl} and R_{ct} changes from faster to slower, indicating the rate of electrochemical corrosion reaction is slowed down. Almost at the same time, the R_{ox} and Q_{ox} begin to appear (Figure 10e,f); this is likely due to a protective cerium film formed on the surface of the substrate, which could retard the corrosion process of the alloy. During the subsequent immersion, both Q_{ox} and R_{ct} gradually increase, which indicates that the corrosion of the aluminum alloy substrate can be effectively inhibited by the cerium-containing film for long time. Compared with the single-layer coating doped with CeTar in the entire coating, the double-layer coating with only CeTar added in the inner layer can also provide similar barrier property and corrosion inhibition for aluminum alloys.

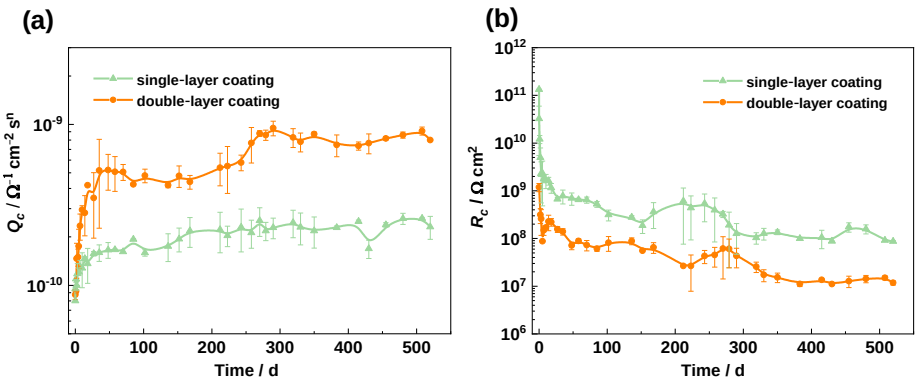

Figure 10. *Cont.*

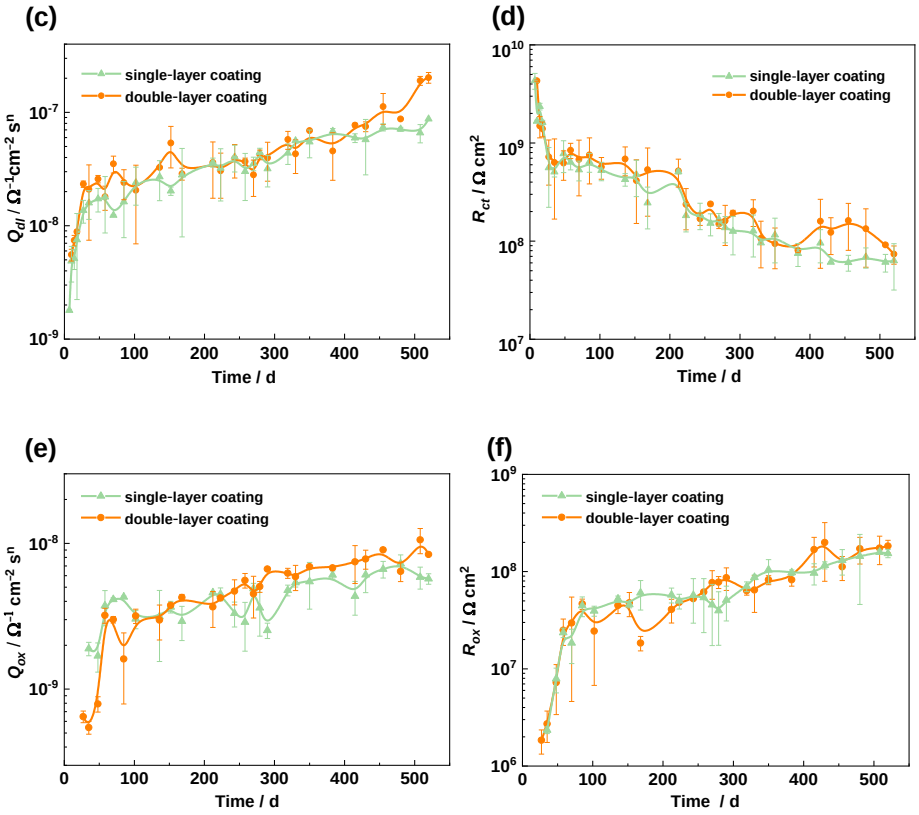

Figure 10. Fitting parameters for two coating samples: (**a**) Q_c; (**b**) R_c; (**c**) Q_{dl}; (**d**) R_{ct}; (**e**) Q_{ox}; (**f**) R_{ox}.

3.4. Cerium Release of the Epoxy Coating

Figure 11 shows the cerium ions release result from the epoxy coating containing 5 wt% CeTar by ICP-MS measurement. Figure 11a shows the amount of cerium ions in the solution detected at different times. After 6 d immersion, the concentration of cerium ions quickly increases to 0.68 μg/(mL·cm^2), and then increases to be slightly slower, which indicates that cerium ions are continuously released form the coating. Figure 11b shows the calculated releasing rate of cerium ions. In the beginning, the cerium ions releasing rate is 0.5 μg/(mL·d·cm^2) and then quickly decreases with time. After 7 d, the release rate decreases to 0.01 μg/(mL·d·cm^2) and then remains basically unchanged. This result is consistent with that in the literature [32]. Based on this, it can be inferred that cerium ions in the coating can also be released constantly towards the interface between the coating and the substrate. The slow continuous releasing of cerium ions to the interface can effectively inhibit the corrosion of the substrate for long time [13].

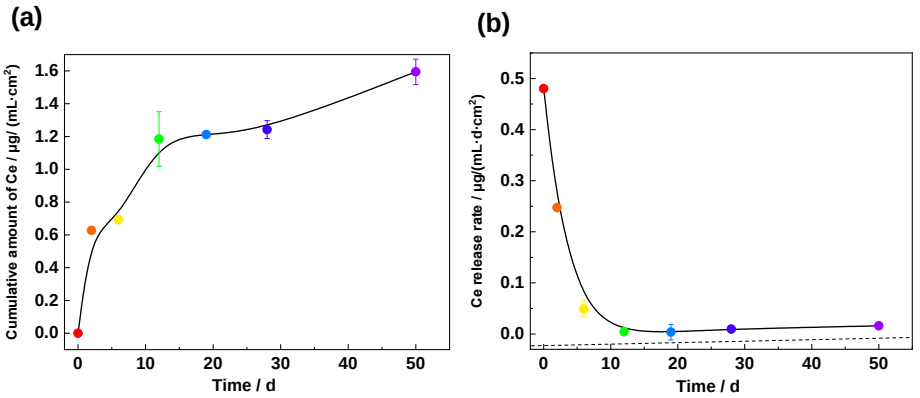

Figure 11. Cerium ions release from the epoxy coatings containing 5 wt% CeTar in 3.5% NaCl solution: (**a**) Cerium ions concentration in the solution; (**b**) Cerium ions release rate.

3.5. FTIR Analysis of the Coatings

In order to study the possible interaction between the cerium tartrate and the epoxy coating, infrared spectroscopy (FTIR) test was performed on the coating. Figure 12 shows the infrared spectra of the coating without and with 5 wt% CeTar before and after immersion for different times, together with that of pure CeTar powder for comparison. In spectrum (a), the peaks at 1601 cm^{-1}, 1561 cm^{-1} and 1385 cm^{-1} can be attributed to the carboxyl (COO−) group of tartaric acid [23,32], and the well-defined shoulder at 1062 cm^{-1} belongs to C−OH bond in CeTar [23]. In spectra (b) and (c), the peaks at 1608 cm^{-1} corresponds to C=C stretch bond, and the peaks in the range of 1511 cm^{-1} to 1034 cm^{-1} (1511 cm^{-1}, 1462 cm^{-1}, 1242 cm^{-1}, 1034 cm^{-1}) are ascribed to the C−H bonds, which are formed in the curing process of epoxy coating [18,33,34]. The peak at 1181 cm^{-1} represents the C−N bond of the amine curing agent, and the peak at 1295 cm^{-1} corresponds to the ether (C−O−C) group [32]. The common peak for all of the coatings at 827 cm^{-1} corresponds to aromatic C−H bending in epoxy coating [32]. Compared with spectra (b) and (c), it also can be seen very clearly in spectrum (f); for the coatings containing 5 wt% CeTar, there is an increase in intensity of the peak at 1113 cm^{-1}, which indicates a possible interaction between CeTar and the polymer and further have effect on the epoxy network structure [13,18,34]. The intensity of the C-N and C-O-C peaks decrease with prolonged immersion time (spectrum (f)), which is related to the release of the curing agent from the coating and the breakage of the epoxy bonds. Meanwhile, the intensity of the characteristic peak of tartaric acid significantly decreases, indicating the release of cerium tartarate (1601 cm^{-1}, 1561 cm^{-1}, 1385 cm^{-1} and 1062 cm^{-1}).

The glass transition temperature (T_g) is closely related with the curing degree of a coating. The T_g of the epoxy coatings without and with 5 wt% CeTar was measured by differential scanning calorimetry (DSC) test [22], which was 60.7 °C and 62.2 °C, respectively. It can be seen that the T_g value of the coating with CeTar is higher than the coating without cerium salts, which means a denser cross-linked network epoxy coating were obtained after CeTar addition. Jouyandeh et al. [19,20] studied the effect of lanthanide-doped Fe_3O_4 nanoparticles on the epoxy curing and also reported similar result. They pointed out that rare earth cations can act as a Lewis acid which facilitate epoxide ring opening by catalyzing the reaction between the epoxy ring and the amine curing agent [19,35].

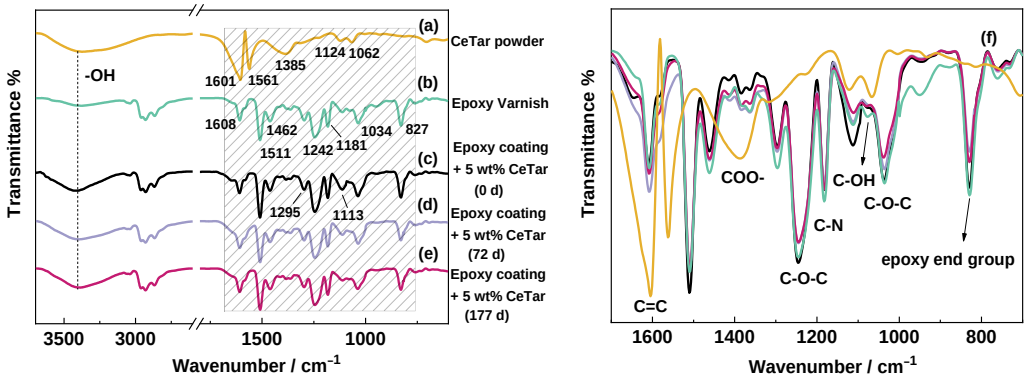

Figure 12. Infrared spectra of (**a**) pure CeTar powder, (**b**) pure epoxy coating, (**c**–**e**) epoxy coating with 5 wt% CeTar before and after immersion for 72 d and 177 d, (**f**) enlarged graph of the wavelength range 1700 cm^{-1}–700 cm^{-1}.

3.6. XPS Analysis Results

In order to study the protective film formed on the aluminum alloy substrate, XPS test was performed after the single-layer and double-layer coatings were removed for 3 d, 5 d, 15 d, 35 d and 520 d, respectively. Firstly, the quantitative analysis of the elements Ce (Ce 3d, around 904 eV, 885 eV, 882 eV and 900 eV) and Cl (Cl 2p, 198 eV) based on the peak areas was performed, and the results are shown in Figure 13. It reveals that the contents of Ce and Cl elements are very low and varied little during the first 15 d of immersion [14,23,36].

After immersion for 35 d, a rapid increase in the contents of Ce and Cl begins to appear on the substrate under both coatings, which indicates that cerium ions have been released from the coating and transfer to the substrate surface along with the electrolyte diffusion, producing a cerium film on the surface. These results confirm the above EIS fitting result, in which the time constants of resistance and capacitance (R_{ox} and Q_{ox}) associated with a protective cerium film starting to occur in EIS spectra after about 30–35 d immersion. At 520 d, the content of cerium further increases, this also can confirm the cerium release is a long-term and continuous process, which could retard the corrosion process of the substrate and effectively enhance the protection of epoxy coating.

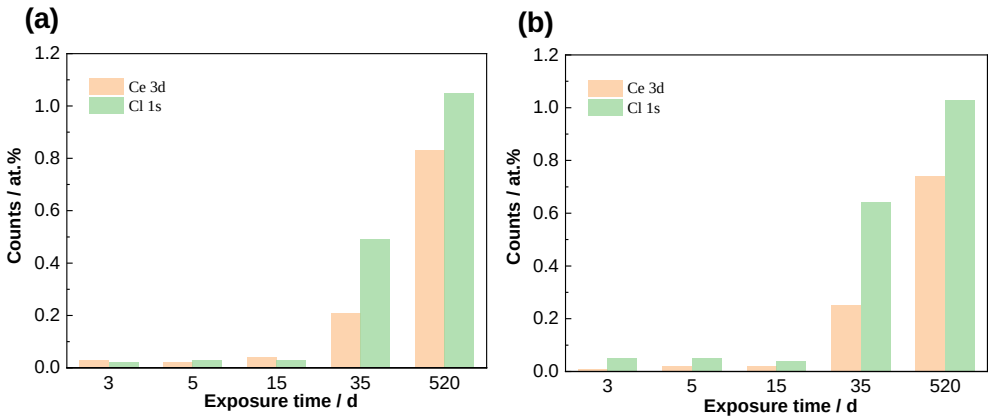

Figure 13. Quantitative analysis of XPS spectra of Al alloy substrate under single-layer coating and double-layer coating immersed in 3.5% NaCl solution for different times: (**a**) single-layer coating; (**b**) double-layer coating.

Figures 14 and 15 show the high-resolution spectra of Ce 3d, O 1s and Al 2p obtained on the Al substrate after the two kinds of coating samples immersion for 35 d and 520 d. The binding energies of 885.8 eV and 904.6 eV are characteristic peaks of Ce(III), 882.3 eV and 900.6 eV indicating the existence of Ce(IV) [14,23,36].The three characteristic peaks obtained at 532.9 eV, 531.9 eV and 531.0 eV represent Ce-O, Al-O and –COO group, respectively [14,36]. These indicate that the protective film detected on the substrate are composed of cerium oxide and hydroxide. The peaks associated to Ce(III) are much higher than those to Ce(IV), suggesting $Ce_2O_3/Ce(OH)_3$ are the dominant species and a small amount of $CeO_2/Ce(OH)_4$ are produced. Besides, the formation of Al-O-CO- by bonding of carboxylic group with Al matrix is detected too, demonstrating the tartaric acid groups in CeTar react with Al^{3+} ions which released into solution from anodic metal dissolution of the matrix to form an insoluble precipitation film containing Al-O-CO-. This precipitation film also has inhibiting action on the corrosion of the substrate [14,23,37]. Therefore, the addition of CeTar to the epoxy coating can supply a synergistic protective effect by tartrate group and cerium ions on the aluminum alloy substrate after immersion for a period of time. The XPS results in Figures 14 and 15 show that there are no apparent difference between the film formed on the substrate under the double-layer coating and single-layer coating. Both would provide excellent protection for the aluminum alloy.

The inhibition mechanism of CeTar in epoxy coating on AA2024-T3 aluminum alloy mainly involves the following aspects. Firstly, cerium ions gradually release form the coating to the substrate after electrolyte enter through the epoxy matrix. Then, the cerium ions react with OH^- ions, which are the cathodic reaction products in cathode areas on the surface, to form cerium hydroxide and oxide films [15,38]. These films could prevent further corrosion of the substrate.

$$O_2 + 2H_2O + 4e \rightarrow OH^- \quad (2)$$

$$Ce^{3+} + 3OH^- \rightarrow Ce(OH)_3\downarrow \quad (3)$$

$$2Ce(OH)_3 \rightarrow Ce_2O_3 + 3H_2O \quad (4)$$

As immersion time prolonged, Ce^{3+} ions are oxidized to Ce^{4+} ions by the action with O_2 and OH^- [38,39], depositing on the surface of Al alloy in the form of intermediate Ce(IV) species, such as $Ce(OH)^{2+}$, and partly convert to more stable state of CeO_2 [40].

$$4Ce^{3+} + O_2 + 4OH^- + 2H_2O \rightarrow 4Ce(OH)^{2+} \quad (5)$$

$$Ce(OH)_2{}^{2+} + 2OH^- \rightarrow CeO_2\downarrow + 2H_2O \quad (6)$$

During the forming process of the cerium oxide/hydroxide film, an insoluble precipitation film containing Al-O-CO- is produced by the reaction between the tartaric acid groups in CeTar and the Al^{3+} ions from the anodic dissolution of the substrate. This also can slow down the corrosion process of the aluminum alloy. Besides, the interaction between CeTar and the polymer matrix also play a positive role in improving the protective property of the coating to some degree. Figure 16 shows the schematic diagram of protection mechanism of the epoxy coating with CeTar on AA2024-T3 aluminum alloy. However, based on a comparison between two-layer and single-layer coating samples, creating a protective film on the substrate could result in a greater contribution.

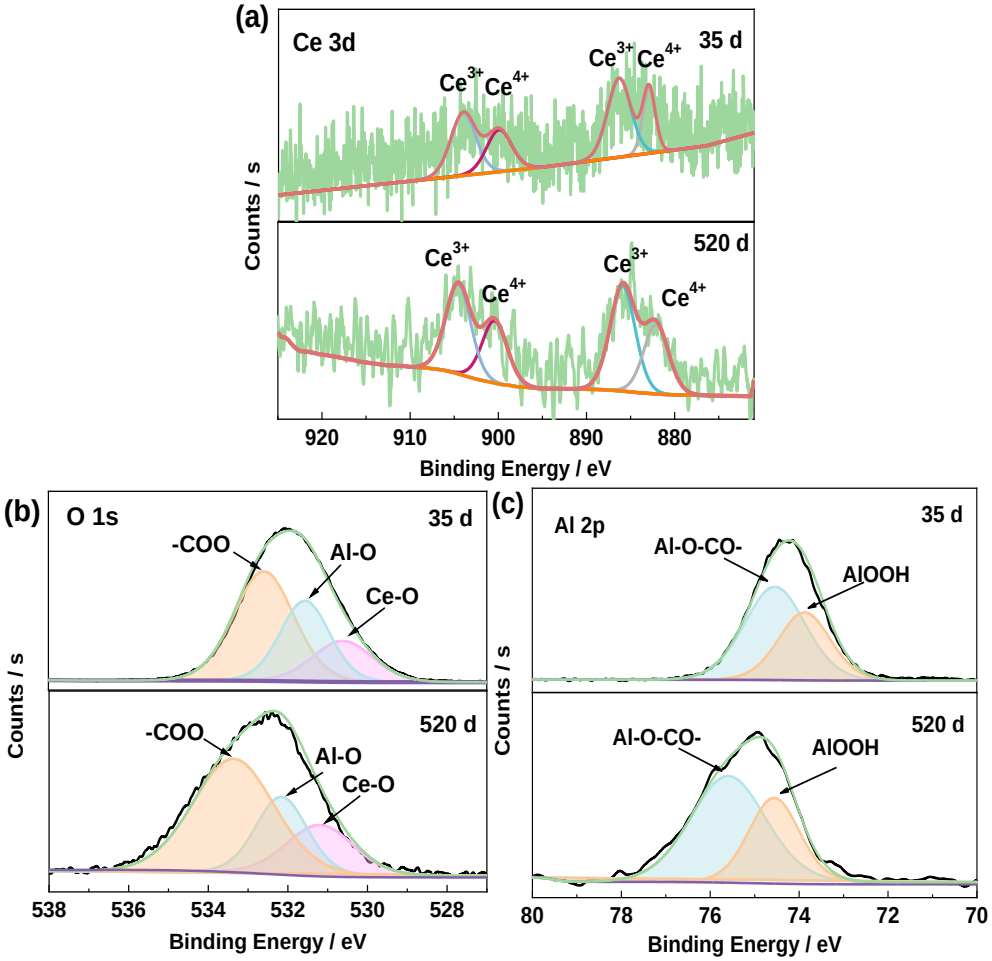

Figure 14. XPS spectra of the substrate surface under double-layer coating immersion in 3.5% NaCl solution for 35 d and 520 d: (**a**) Ce 3d; (**b**) O 1s; (**c**) Al 2p.

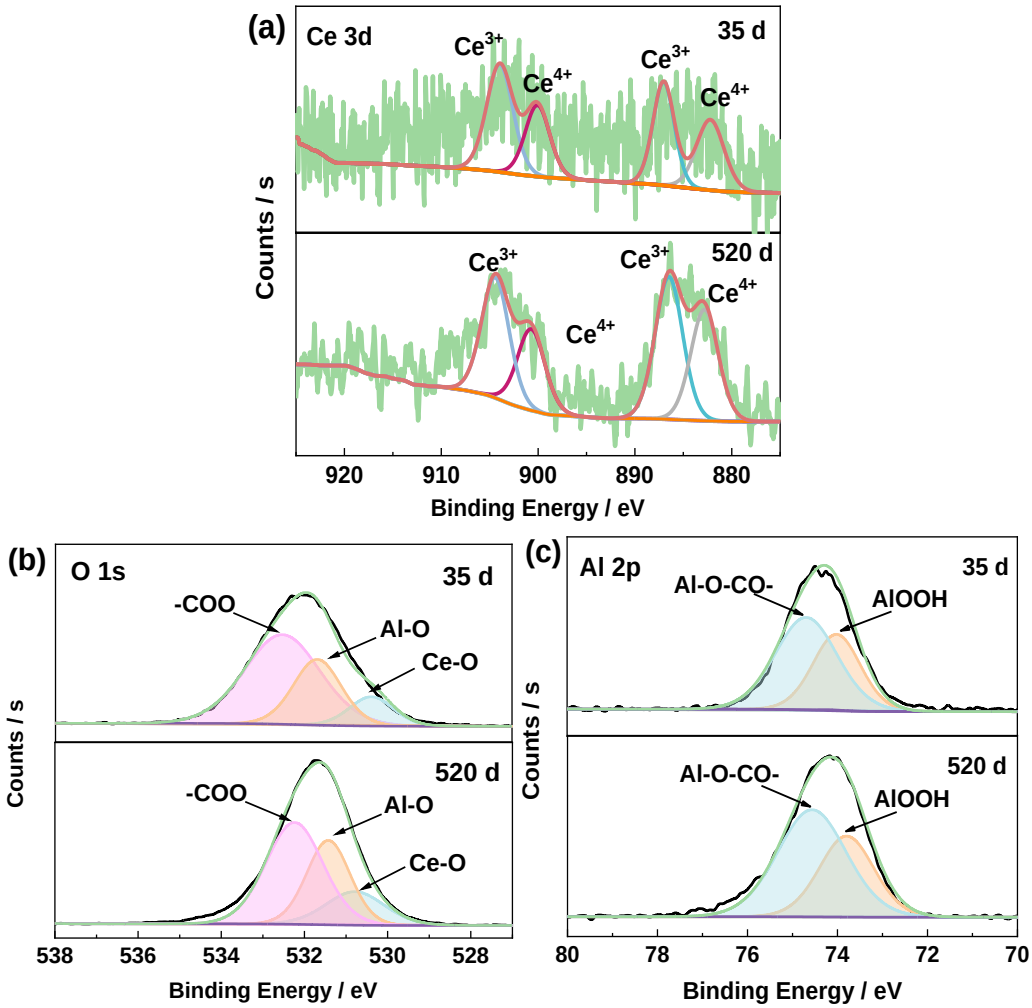

Figure 15. XPS spectra of the substrate surface under single-layer coating after immersion in 3.5% NaCl solution for 35 d and 520 d: (**a**) Ce 3d; (**b**) O 1s; (**c**) Al 2p.

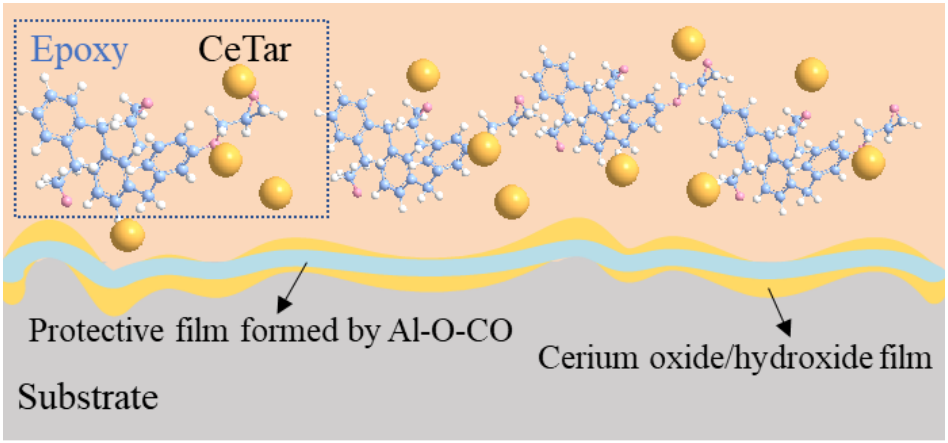

Figure 16. Schematic diagram of protection mechanism of the epoxy coating with CeTar on aluminum alloy.

4. Conclusions

(1) The addition of 5 wt% cerium tartrate (CeTar) can significantly improve the protective property of the epoxy coating to AA2024-T3 aluminum alloy in 3.5% NaCl solution for longer than 520 d;

(2) After continuously releasing to the coating/alloy interface, the CeTar can supply a synergistic inhibitory effect of tartrate group and cerium ions on the aluminum alloy substrate, forming a cerium-containing oxide/hydroxide film and insoluble precipitation film. In addition, the CeTar has a positive effect on the network structure of the epoxy coating;

(3) The double-layer epoxy coating in which only the inner layer loaded with 5 wt% CeTar provide similar protective performance to the single-layer epoxy coating containing 5 wt% CeTar entirely. Based on the comparison of these two coatings, creating a protective film on the substrate could result in a greater contribution. In other words, the protective property of epoxy coating has close relationship with the hindering effect on the corrosion process of the aluminum alloy by the protective film.

Author Contributions: Writing—original draft and investigation, X.C. and J.T.; Characterization and data analysis, H.W.; Methodology and data analysis guiding, H.Z.; Supervision, Writing—review and editing, Y.T.; Methodology, Writing—review and editing, X.Z. and Y.Z. All authors have read and agreed to the published version of the manuscript.

Funding: This research received no external funding.

Institutional Review Board Statement: Not applicable.

Informed Consent Statement: Not applicable.

Data Availability Statement: Not applicable.

Conflicts of Interest: The authors declare no conflict of interest.

References

1. Huda, Z.; Taib, N.I.; Zaharinie, T. Characterization of 2024-T3: An aerospace aluminum alloy. *Mater. Chem. Phys.* **2009**, *113*, 515–517. [CrossRef]
2. Nawaz, M.; Shakoor, R.A.; Kahraman, R.; Montemor, M.F. Cerium oxide loaded with Gum Arabic as environmentally friendly anti-corrosion additive for protection of coated steel. *Mater. Des.* **2021**, *198*, 109361. [CrossRef]
3. Vakili, H.; Ramezanzadeh, B.; Amini, R. The corrosion performance and adhesion properties of the epoxy coating applied on the steel substrates treated by cerium-based conversion coatings. *Corros. Sci.* **2015**, *94*, 466–475. [CrossRef]
4. Wang, Y.F.; Su, H.; Gu, Y.L.; Song, X.; Zhao, J.S. Carcinogenicity of chromium and chemoprevention: A brief update. *OncoTargets Ther.* **2017**, *10*, 4065–4079. [CrossRef]
5. Hinton, B.R.W.; Arnott, D.R.; Ryan, N.E. Inhibition of aluminum alloy corrosion by cerous cations. *Met. Forum* **1984**, *7*, 211–217.
6. Hinton, B.R.W. Corrosion inhibition with rare earth metal salts. *J. Alloy. Compd.* **1992**, *180*, 15–25. [CrossRef]
7. Deyab, M.A.; El-Rehim, S.S.A.; Hassan, H.H.; Shaltot, A.M. Impact of rare earth compounds on corrosion of aluminum alloy (AA6061) in the marine water environment. *J. Alloy. Compd.* **2020**, *820*, 153428. [CrossRef]
8. Mishra, A.K.; Balasubramaniam, R. Corrosion inhibition of aluminum alloy AA2014 by rare earth chlorides. *Corro. Sci.* **2007**, *49*, 1027–1044. [CrossRef]
9. Zhao, D.; Sun, J.; Zhang, L.L.; Tan, Y.; Li, J. Corrosion behavior of rare earth cerium based conversion coating on aluminum alloy. *J. Rare Earths.* **2010**, *28*, 371–374. [CrossRef]
10. Yasakau, K.; Zheludkevich, M.L.; Lamaka, S.V.; Ferreira, M.G.S. Mechanism of corrosion inhibition of AA2024 by rare-earth compounds. *J. Phys. Chem. B* **2006**, *110*, 5515–5528. [CrossRef]
11. Ho, D.; Brack, N.; Scully, J.; Markley, T.; Forsyth, M.; Hinton, B.R.W. Cerium dibutylphosphate as a corrosion inhibitor for AA2024-T3 aluminum alloys. *J. Electrochem. Soc.* **2006**, *153*, B392–B401. [CrossRef]
12. Xhanari, K.; Finšgar, M. Organic corrosion inhibitors for aluminum and its alloys in chloride and alkaline solutions: A review. *Arab. J. Chem.* **2019**, *12*, 4646–4663. [CrossRef]
13. Tiringer, U.; Durán, A.; Castro, Y.; Milošev, I. Self-healing effect of hybrid sol-gel coatings based on GPTMS, TEOS, SiO_2 nanoparticles and $Ce(NO_3)_3$ applied on aluminum alloy 7075-T6. *J. Electrochem. Soc.* **2018**, *165*, C213–C225. [CrossRef]
14. Shi, H.W.; Han, E.-H.; Liu, F.C. Corrosion protection of aluminium alloy 2024-T3 in 0.05 M NaCl by cerium cinnamate. *Corros. Sci.* **2011**, *53*, 2374–2384. [CrossRef]
15. Shi, H.W.; Han, E.-H.; Lamaka, S.V.; Zheludkevich, M.L.; Liu, F.; Ferreira, M.G.S. Cerium cinnamate as an environmentally benign inhibitor pigment for epoxy coatings on AA2024-T3. *Prog. Org. Coat.* **2014**, *77*, 765–773. [CrossRef]
16. Soestbergen, M.V.; Baukh, V.; Erich, S.J.F.; Huinink, H.P.; Adan, O.C.G. Release of cerium dibutylphosphate corrosion inhibitors from highly filled epoxy coating systems. *Prog. Org. Coat.* **2014**, *77*, 1562–1568. [CrossRef]
17. Gobara, M.; Baraka, A.; Akid, R.; Zorainy, M. Corrosion protection mechanism of Ce^{4+}/organic inhibitor for AA2024 in 3.5% NaCl. *RSC Adv.* **2020**, *10*, 2227–2240. [CrossRef] [PubMed]

18. Mardel, J.; Garcia, S.J.; Corrigan, P.A.; Markley, T.; Hughes, A.E.; Muster, T.H.; Lau, D.; Harvey, T.G.; Glenn, A.M.; White, P.A.; et al. The characterisation and performance of Ce(dbp)$_3$-inhibited epoxy coatings. *Prog. Org. Coat.* **2011**, *70*, 91–101. [CrossRef]
19. Jouyandeh, M.; Ganjali, M.R.; Mehrpooya, M.; Abida, O.; Jabbour, K.; Rabiee, N.; Habibzadeh, S.; Mashahdzadeh, A.H.; García-Peñas, A.; Stadler, F.J.; et al. Cure kinetics of samarium-doped Fe_3O_4 epoxy nanocomposites. *J. Compos. Sci.* **2022**, *6*, 29. [CrossRef]
20. Jouyandeh, M.; Ganjali, M.R.; Ali, J.A.; Akbari, V.; Karami, Z.; Aghazadeh, M.; Zarrintaj, P.; Saeb, M.R. Curing epoxy with polyethylene glycol (PEG) surface-functionalized $GdxFe_{3-x}O_4$ magnetic nanoparticles. *Prog. Org. Coat.* **2019**, *137*, 105283. [CrossRef]
21. Jouyandeh, M.; Zarrintaj, P.; Ganjali, M.R.; Ali, J.A.; Karimzadeh, I.; Aghazadeh, M.; Ghaffari, M.; Saeb, M.R. Curing epoxy with electrochemically synthesized $GdxFe_{3-x}O_4$ magnetic nanoparticles. *Prog. Org. Coat.* **2019**, *136*, 105245. [CrossRef]
22. Hu, T.H.; Shi, H.W.; Fan, S.H.; Liu, F.C.; Han, E.-H. Cerium tartrate as a pigment in epoxy coatings for corrosion protection of AA2024-T3. *Prog. Org. Coat.* **2017**, *105*, 123–131. [CrossRef]
23. Hu, T.H.; Shi, H.W.; Wei, T.; Liu, F.C.; Fan, S.H.; Han, E.-H. Cerium tartrate as a corrosion inhibitor for AA2024-T3. *Corros. Sci.* **2015**, *95*, 152–161. [CrossRef]
24. Wei, H.; Tang, J.H.; Chen, X.P.; Tang, Y.M.; Zhao, X.H.; Zuo, Y. Influence of organic and inorganic cerium salts on the protective performance of epoxy coating. *Prog. Org. Coat.* **2022**, *166*, 106763. [CrossRef]
25. Zhu, R.L.; Zhang, J.; Chang, C.; Gao, S.; Ni, N. Effect of silane and zirconia on the thermal property of cathodic electrophoretic coating on AZ31 magnesium alloy. *J. Magnes. Alloy.* **2013**, *1*, 235–241. [CrossRef]
26. Zhu, D.; van Ooij, W.J. Corrosion protection of metals by water-based silanemixtures of bis-[trimethoxysilylpropyl] amine and vinyltriacetoxysilane. *Prog. Org. Coat.* **2004**, *49*, 42–53. [CrossRef]
27. Feng, X.G.; Zhu, C.; Lu, X.Y.; Zhang, Y.J.; Wu, T.; Zuo, Y.; Zhao, X.H.; Dun, Y.C.; Wang, M. The influence of hydrofluoric acid doped polyaniline on the protective performance of a Mg-rich epoxy coating on AZ91D magnesium alloy. *Prog. Org. Coat.* **2020**, *141*, 105550. [CrossRef]
28. Ji, W.-G.; Hu, J.-M.; Liu, L.; Zhang, J.-Q.; Cao, C.-N. Enhancement of corrosion performance of epoxy coatings by chemical modification with GPTMS silane monomer. *J. Adhes. Sci. Technol.* **2008**, *22*, 77–92. [CrossRef]
29. *GB/T 6824-2008*; Determination for release rate of cupper-ion for antifouling paint on ship bottom. GB/T: Beijing, China, 2008. (In Chinese)
30. Sun, W.; Xing, C.; Tang, X.B.; Zuo, Y.; Tang, Y.M.; Zhao, X.H. Comparative study on the degradation of a zinc-rich epoxy primer/acrylic polyurethane coating in different simulated atmospheric solutions. *J. Coat. Technol. Res.* **2021**, *18*, 397–413. [CrossRef]
31. Xing, C.; Wang, W.; Qu, S.; Tang, Y.M.; Zhao, X.H.; Zuo, Y. Degradation of Zinc-rich epoxy coating in 3.5% NaCl solution and evolution of its EIS parameters. *J. Coat. Technol. Res.* **2021**, *18*, 843–860. [CrossRef]
32. Peng, Y.; Hughes, A.E.; Mardel, J.I.; Deacon, G.B.; Junk, P.C.; Forsyth, M.; Hinton, B.R.W.; Somers, A.E. Leaching behavior and corrosion inhibition of a rare earth carboxylate incorporated epoxy coating system. *ACS Appl. Mater. Interfaces* **2019**, *11*, 36154–36168. [CrossRef]
33. Ubaid, F.; Naeem, N.; Shakoor, R.A.; Kahraman, R.; Mansour, S.; Zekri, A. Effect of concentration of DOC loaded TiO_2 nanotubes on the corrosion behavior of smart coatings. *Ceram. Int.* **2019**, *45*, 10492–10500. [CrossRef]
34. Jegdić, B.V.; Živković, L.S.; Popić, J.P.; Rogan, J.; Bajat, J.B.; Mišković-Stanković, V.B. Corrosion stability of cerium-doped cataphoretic epoxy coatings on AA6060 alloy. *Mater. Corros.* **2016**, *67*, 1173–1184. [CrossRef]
35. Jouyandeh, M.; Paran, S.M.R.; Khadem, S.S.M.; Ganjali, M.R.; Akbari, V.; Vahabi, H.; Saeb, M.R. Nonisothermal cure kinetics of epoxy/$Mn_xFe_{3-x}O_4$ nanocomposites. *Prog. Org. Coat.* **2020**, *140*, 105505. [CrossRef]
36. Dabalà, M.; Armelao, L.; Buchberger, A.; Calliari, I. Cerium-based conversion layers on aluminum alloys. *Appl. Surf. Sci.* **2001**, *172*, 312–322. [CrossRef]
37. Alexander, M.R.; Beamson, G.; Blomfield, C.J.; Leggett, G.; Duc, T.M. Interaction of carboxylic acids with the oxyhydroxide surface of aluminium: Poly(acrylic acid), acetic acid and propionic acid on pseudoboehmite. *J. Electron. Spectrosc. Relat. Phenom.* **2001**, *121*, 19–32. [CrossRef]
38. Saei, E.; Ramezanzadeh, B.; Amini, R.; Kalajahik, M.S. Effects of combined organic and inorganic corrosion inhibitors on the nanostructure cerium based conversion coating performance on AZ31 magnesium alloy: Morphological and corrosion studies. *Corro. Sci.* **2017**, *127*, 186–200. [CrossRef]
39. Pu, Y.; Hayes, S.A.; O'Keefe, T.J.; O'Keefe, M.J.; Stoffer, J.O. The phase stability of cerium species in aqueous systems. *J. Electrochem. Soc.* **2006**, *153*, C74–C79. [CrossRef]
40. Ramezanzadeh, B.; Rostami, M. The effect of cerium-based conversion treatment on the cathodic delamination and corrosion protection performance of carbon steel-fusion-bonded epoxy coating systems. *Appl. Surf. Sci.* **2017**, *392*, 1004–1016. [CrossRef]